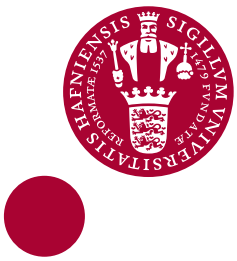

Matrix Polysaccharides and SiaD Diguanylate Cyclase Alter Community Structure and Competitiveness of Pseudomonas aeruginosa during Dual-Species Biofilm Development with Staphylococcus aureus

Chew, Su Chuen; Yam, Joey Kuok Hoong; Matysik, Artur; Seng, Zi Jing; Klebensberger, Janosch; Givskov, Michael; Doyle, Patrick; Rice, Scott A.; Yang, Liang; Kjelleberg, Staffan

Published in:
mBio

DOI:
10.1128/mBio.00585-18

Publication date:
2018

Document version
Publisher's PDF, also known as Version of record

AMERICAN SOCIETY FOR MICROBIOLOGY | mBio®

RESEARCH ARTICLE
Molecular Biology and Physiology

Matrix Polysaccharides and SiaD Diguanylate Cyclase Alter Community Structure and Competitiveness of *Pseudomonas aeruginosa* during Dual-Species Biofilm Development with *Staphylococcus aureus*

Su Chuen Chew,[a,b] Joey Kuok Hoong Yam,[a] Artur Matysik,[a] Zi Jing Seng,[a] Janosch Klebensberger,[c] Michael Givskov,[a,d] Patrick Doyle,[b,e] Scott A. Rice,[a,f,g] Liang Yang,[a,f] Staffan Kjelleberg[a,f,h]

[a]Singapore Centre for Environmental Life Sciences Engineering (SCELSE), Nanyang Technological University, Singapore

[b]Singapore-MIT Alliance for Research and Technology, Singapore

[c]University of Stuttgart, Institute of Biochemistry and Technical Biochemistry, Stuttgart, Germany

[d]Costerton Biofilm Center, Department of International Health, Immunology and Microbiology, University of Copenhagen, Copenhagen, Denmark

[e]Department of Chemical Engineering, Massachusetts Institute of Technology, Cambridge, Massachusetts, USA

[f]School of Biological Sciences, Nanyang Technological University, Singapore

[g]The ithree Institute, The University of Technology Sydney, Sydney, Australia

[h]Center for Marine Bio-Innovation and School of Biotechnology and Biomolecular Sciences, University of New South Wales, Sydney, Australia

ABSTRACT Mixed-species biofilms display a number of emergent properties, including enhanced antimicrobial tolerance and communal metabolism. These properties may depend on interspecies relationships and the structure of the biofilm. However, the contribution of specific matrix components to emergent properties of mixed-species biofilms remains poorly understood. Using a dual-species biofilm community formed by the opportunistic pathogens *Pseudomonas aeruginosa* and *Staphylococcus aureus*, we found that whilst neither Pel nor Psl polysaccharides, produced by *P. aeruginosa*, affect relative species abundance in mature *P. aeruginosa* and *S. aureus* biofilms, Psl production is associated with increased *P. aeruginosa* abundance and reduced *S. aureus* aggregation in the early stages of biofilm formation. Our data suggest that the competitive effect of Psl is not associated with its structural role in cross-linking the matrix and adhering to *P. aeruginosa* cells but is instead mediated through the activation of the diguanylate cyclase SiaD. This regulatory control was also found to be independent of the siderophore pyoverdine and *Pseudomonas* quinolone signal, which have previously been proposed to reduce *S. aureus* viability by inducing lactic acid fermentation-based growth. In contrast to the effect mediated by Psl, Pel reduced the effective crosslinking of the biofilm matrix and facilitated superdiffusivity in microcolony regions. These changes in matrix cross-linking enhance biofilm surface spreading and expansion of microcolonies in the later stages of biofilm development, improving overall dual-species biofilm growth and increasing biovolume severalfold. Thus, the biofilm matrix and regulators associated with matrix production play essential roles in mixed-species biofilm interactions.

IMPORTANCE Bacteria in natural and engineered environments form biofilms that include many different species. Microorganisms rely on a number of different strategies to manage social interactions with other species and to access resources, build biofilm consortia, and optimize growth. For example, *Pseudomonas aeruginosa* and *Staphylococcus aureus* are biofilm-forming bacteria that coinfect the lungs of cystic

Received 25 September 2018 **Accepted** 28 September 2018 **Published** 6 November 2018

Citation Chew SC, Yam JKH, Matysik A, Seng ZJ, Klebensberger J, Givskov M, Doyle P, Rice SA, Yang L, Kjelleberg S. 2018. Matrix polysaccharides and SiaD diguanylate cyclase alter community structure and competitiveness of *Pseudomonas aeruginosa* during dual-species biofilm development with *Staphylococcus aureus*. mBio 9:e00585-18. https://doi.org/10.1128/mBio.00585-18.

Editor Edward G. Ruby, University of Hawaii at Manoa

Address correspondence to Liang Yang, yangliang@ntu.edu.sg, or Staffan Kjelleberg, LASKjelleberg@ntu.edu.sg.

This article is a direct contribution from a Fellow of the American Academy of Microbiology. Solicited external reviewers: Miguel Cámara, University of Nottingham; Ehud Banin, Bar-Ilan University; Paul Stoodley, The Ohio State University.

fibrosis patients and diabetic and chronic wounds. *P. aeruginosa* is known to antagonize *S. aureus* growth. However, many of the factors responsible for mixed-species interactions and outcomes such as infections are poorly understood. Biofilm bacteria are encased in a self-produced extracellular matrix that facilitates interspecies behavior and biofilm development. In this study, we examined the poorly understood roles of the major matrix biopolymers and their regulators in mixed-species biofilm interactions and development.

KEYWORDS *Pseudomonas aeruginosa*, SiaD, *Staphylococcus aureus*, biofilms, cyclic di-GMP, exopolysaccharide, microrheology

Bacteria exist predominantly as dense, self-organized communities encased in self-produced matrices known as biofilms (1, 2). They exhibit emergent properties that are not found in their single-cell planktonic counterparts, such as altered and enhanced metabolic efficiency (3–5), increased robustness and resistance to antimicrobial attack (6, 7), altered virulence (8, 9), and enhanced horizontal gene transfer (10, 11). These emergent properties contribute to their roles in the Earth's natural cycling of nitrogen and sulfur and of many metals (12–14) as well as in survival in host organisms, where they can live as commensals or as pathogens (14). While biofilms usually encompass a large diversity of bacterial species that have synergistic, mutualistic, competitive, or antagonistic relationships, the fundamental mechanisms that drive mixed-species biofilm development and the associated emergent properties remain poorly understood.

Pseudomonas aeruginosa and *Staphylococcus aureus* are opportunistic pathogens found in infections of cystic fibrosis (CF) lungs and in diabetic and chronic wounds (14, 15). Such mixed-species infections are correlated with poor clinical outcomes (16); hence, the two organisms serve as a model dual-species community to represent polymicrobial infections (17, 18). The two bacterial species are known to have an antagonistic relationship, where *P. aeruginosa* produces heptyl-4-hydroxyquinoline N-oxide (HQNO), a potent inhibitor of respiratory electron transfer and a component of its *Pseudomonas* quinolone signal (PQS) system, to kill *S. aureus* (19). However, this also selects for *S. aureus* small-colony variants (SCVs) that have mutations in the electron transport chain and increased resistance to *P. aeruginosa* killing (20). This has an impact on disease prognosis, as the prevalence of *S. aureus* SCVs is correlated with a more severe disease state (16). *P. aeruginosa* also induces the production of the host enzyme sPLA2-IIA to kill *S. aureus* (21). While these two species serve as a model system for polymicrobial infections, the mechanisms of interaction during dual-species biofilm formation has been less extensively explored.

P. aeruginosa is known to express three polysaccharides, alginate, Pel, and Psl, as the major matrix components (22). *P. aeruginosa* isolates from the cystic fibrosis (CF) lung environment tend to become mucoid through overexpression of alginate (23). However, only Pel and Psl have been shown to be required for biofilm formation (24, 25). Psl is important for surface attachment (24, 26, 27), autoaggregative phenotypes in batch cultures (28–30), and activation of specific enzymes (diguanylate cyclases [DGCs]) to increase intracellular levels of cyclic-di-GMP, triggering *P. aeruginosa* to enter the biofilm mode of life (31, 32). Thus, the loss of Psl results in delayed biofilm development and either a delay in or loss of microcolony formation (25, 26, 33). Pel is often associated with the formation of floating biofilms (pellicles) and plays a role in biofilm maturation (24, 26, 33). Pel and Psl have different mechanical properties and resistances to flow that result in differences in biofilm structure and development (33). In mucoid *P. aeruginosa-S. aureus* biofilms, Psl expression led to *P. aeruginosa* exclusively occupying the upper layer of biofilms, whereas Pel expression appeared to increase colocalization of *P. aeruginosa* and *S. aureus* (33).

Recently, it was found that protein A, a cell wall protein of *S. aureus*, binds to the Psl polysaccharide and type IV pili in *P. aeruginosa* to inhibit biofilm formation (34). The Psl polysaccharide is also known to affect the community structure and stress resistance, where it confers antibiotic protection to the *Escherichia coli-S. aureus* biofilm commu-

TABLE 1 List of bacterial strains[a]

Strain	Relevant characteristic(s)	Reference or source
P. aeruginosa wtPAO1	Wild-type strain	64
P. aeruginosa Δ*pelA*	PAO1 that does not produce the Pel matrix polysaccharide	53
P. aeruginosa Δ*pslBCD*	PAO1 that does not express the Psl matrix polysaccharide	53
P. aeruginosa Δ*cdrA*	PAO1 lacking the extracellular adhesin CdrA	This study
P. aeruginosa Δ*sadC*	PAO1 lacking the DGC SadC	51
P. aeruginosa Δ*siaD*	PAO1 lacking the DGC SiaD	51
P. aeruginosa Δ*siaD*/pUC18-*siaD*	Carb^r; ΔSiaD mutant containing the pUC18-*siaD* complementation plasmid	This study
S. aureus 15981	Wild-type strain	53

[a]wtPAO1, wild-type strain PAO1; Carb^r, carboxylate resistance.

nity (35), as well as increased *P. aeruginosa* abundance and SDS tolerance of three-species biofilms of *P. aeruginosa*, *Pseudomonas protegens*, and *Klebsiella pneumoniae* (36). Thus, the composition of the biofilm matrix represents an important and yet largely underexplored mediator of interspecies interactions and confers emergent properties to the community.

To address how Pel and Psl affect *P. aeruginosa* competitiveness, biofilm structure, and rheology in mixed-species biofilm communities, we established dual-species biofilms of *P. aeruginosa* and *S. aureus*. We explored the importance of the structural role of Psl in the biofilm matrix through analysis of the adhesin CdrA, which physically binds *P. aeruginosa* cells to the Psl matrix (28), and the regulatory role of Psl in biofilm formation through analysis of the diguanylate cyclases SadC and SiaD, which are activated by Psl to increase c-di-GMP levels (31, 32). In this study, we demonstrate that Psl enables wild-type *P. aeruginosa* to outcompete *S. aureus* in early biofilm development and that SiaD is necessary for *P. aeruginosa* to outcompete *S. aureus* in a pyoverdine- and PQS-independent manner. In late-stage biofilm development, the production of Pel is required to reduce the effective cross-linking of the matrix to increase the spreading surface coverage of *P. aeruginosa* in dual-species biofilms.

RESULTS

The accumulation of *P. aeruginosa* in mixed biofilms with *S. aureus* is facilitated by Psl during early biofilm formation whereas Pel mediates biofilm maturation. mCherry-tagged, wild-type *P. aeruginosa* PAO1 or its isogenic Pel and Psl mutants (Table 1) was cocultivated with Gfp-tagged wild-type *S. aureus* 15981 to examine the impact of the matrix polysaccharides Pel and Psl on the development of *P. aeruginosa-S. aureus* biofilms (Fig. 1). Wild-type monospecies biofilms, seeded with the same total cell densities as the dual-species biofilms, were also formed for comparison to wild-type dual-species biofilms. The biovolume of each species in the biofilms was calculated using COMSTAT (Table 2). At 1 h, the monospecies wild-type biofilms had total biovolumes of 26,286 ± 4,128 μm^3 mm^{-2} (*P. aeruginosa*) and 39,168 ± 2,660 μm^3 mm^{-2} (*S. aureus*). This was similar to the results seen with dual-species biofilms with a total biovolume of 28,419 ± 4,586 μm^3 mm^{-2}, where the two species were present in approximately equal amounts. For monospecies wild-type *P. aeruginosa*, the highest biovolume of 1,548,912 ± 682,644 μm^3 mm^{-2} was reached at 13 h and decreased to 277,455 ± 292,722 μm^3 mm^{-2} at 19 h. Monospecies wild-type *S. aureus* had lower biovolumes (851,130 ± 292,722 μm^3 mm^{-2}) than monospecies wild-type *P. aeruginosa* at 13 h, but its biovolumes increased to 4,068,969 ± 1,335,431 μm^3 mm^{-2} by 19 h.

For dual-species wild-type *P. aeruginosa-S. aureus*, the highest total biovolume was 850,128 ± 113,105 μm^3 mm^{-2} at 13 h, with *S. aureus* comprising only 1.5% or 12,785 μm^3 mm^{-2} of the biovolume. These biovolume levels were unchanged at 19 h, which contrasts with the monospecies biofilms of *P. aeruginosa*. This would suggest that *P. aeruginosa* biofilms persist longer in the presence of *S. aureus*. *S. aureus* made up a minor portion of biovolumes in the dual-species biofilm and reached a peak biovolume of 35,015 ± 18,203 μm^3 mm^{-2} at 7 h, in contrast to the biovolume seen when it was

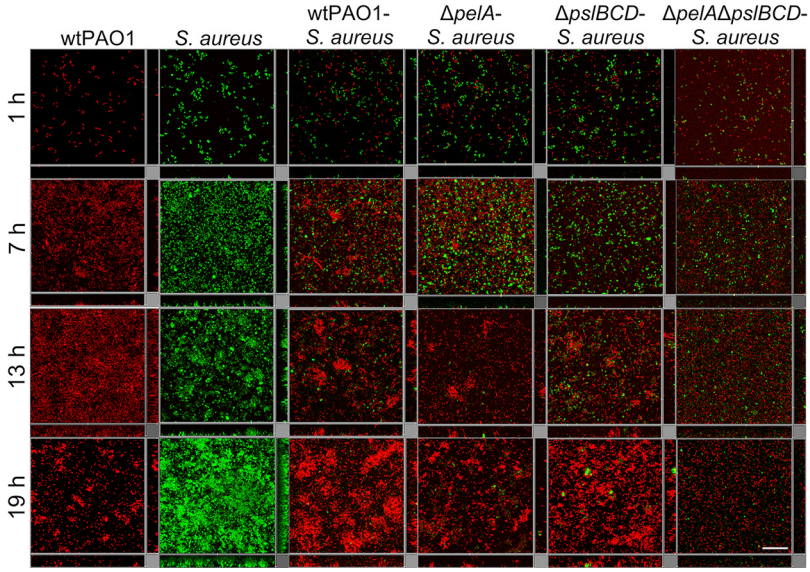

FIG 1 The development of 19-h wild-type *P. aeruginosa-S. aureus*, *P. aeruginosa* Δ*pelA-S. aureus*, and *P. aeruginosa* Δ*pslBCD-S. aureus* dual-species biofilms imaged using confocal imaging every 6 h. The monospecies wild-type *P. aeruginosa* and *S. aureus* biofilms are shown for comparison. *P. aeruginosa* is mCherry tagged (red), and *S. aureus* is Gfp tagged (green). Images are representative of four biological replicates. The scale bar is 30 μm.

grown as a monospecies biofilm (495,781 ± 190,117 μm^3 mm^{-2}). This indicates that *P. aeruginosa* inhibited *S. aureus* growth during early biofilm development.

For all dual-species *P. aeruginosa-S. aureus* biofilms, the biovolume of *P. aeruginosa* was roughly equal to the biovolume of *S. aureus* in the initial phase of biofilm formation (i.e., after 1 h of inoculation). The average biovolume for each species ranged from 13,045 to 17,662 μm^3 mm^{-2}, with the exception of mutant Δ*pelA* Δ*pslBCD-S. aureus* biofilms, where each species displayed approximately half those biovolumes (Fig. 2A) (Table 2).

During dual-species biofilm development, the average biovolume for both wild-type *P. aeruginosa* and the Δ*pelA* mutant increased by approximately 5-fold during the first 7 h. The average biovolume of wild-type *P. aeruginosa* increased by 10-fold at 13 h and remained relatively constant at 792,562 ± 10,272 μm^3 mm^{-2} at 19 h. The Δ*pelA* mutant increased in biovolume by 3-fold to 4-fold between 7 and 13 h and remained constant

TABLE 2 Biovolumes for single- and dual-species biofilms[a]

Biofilm	Strain(s)	Biovolume per area (μm^3 mm^{-2})			
		1 h	7 h	13 h	19 h
Monospecies: *P. aeruginosa*	wtPAO1	26,286 ± 4,128	542,412 ± 260,428	1,548,912 ± 682,644	277,455 ± 59,146
Monospecies: *S. aureus*	*S. aureus* 15981	39,168 ± 2,660	495,781 ± 190,117	851,130 ± 292,722	4,068,969 ± 1,335,431
Dual species: *P. aeruginosa-S. aureus*	wtPAO1	14,388 ± 2,168	73,488 ± 21,746	837,343 ± 104,916	792,562 ± 10,272
	S. aureus 15981	14,031 ± 2,418	35,015 ± 18,203	12,785 ± 8,189	10,521 ± 3,878
Dual species: mutant Δ*pelA-S. aureus*	Mutant Δ*pelA*	14,285 ± 2,693	82,682 ± 32,691	220,077 ± 52,939*	267,374 ± 114,530*
	S. aureus 15981	13,045 ± 1,993	128,861 ± 62,036	6,927 ± 2,785	14,982 ± 4,887
Dual species: mutant Δ*pslBCD-S. aureus*	Mutant Δ*pslBCD*	14,722 ± 799	14,992 ± 4,185	178,387 ± 48,490*	1,419,718 ± 432,200
	S. aureus 15981	17,662 ± 1,729	62,035 ± 15,636	67,605 ± 31,815	20,726 ± 5,301
Dual species: mutant Δ*pelA* Δ*pslBCD-S. aureus*	Mutant Δ*pelA* Δ*pslBCD*	7,611 ± 513*	23,988 ± 2,379	21,310 ± 4,559*	50,401 ± 21,795*
	S. aureus 15981	7,691 ± 2,315	17,752 ± 5,103	4,559 ± 1,818	1,868 ± 701

[a]Data represent results from four biological replicates with each replicate composed of three confocal images of the biofilm in different areas on average. Asterisks (*) indicate a significant difference from the wild-type *P. aeruginosa-S. aureus* biofilms ($P < 0.05$) (unpaired *t* test with Welch's correction). Error data represent SEM.

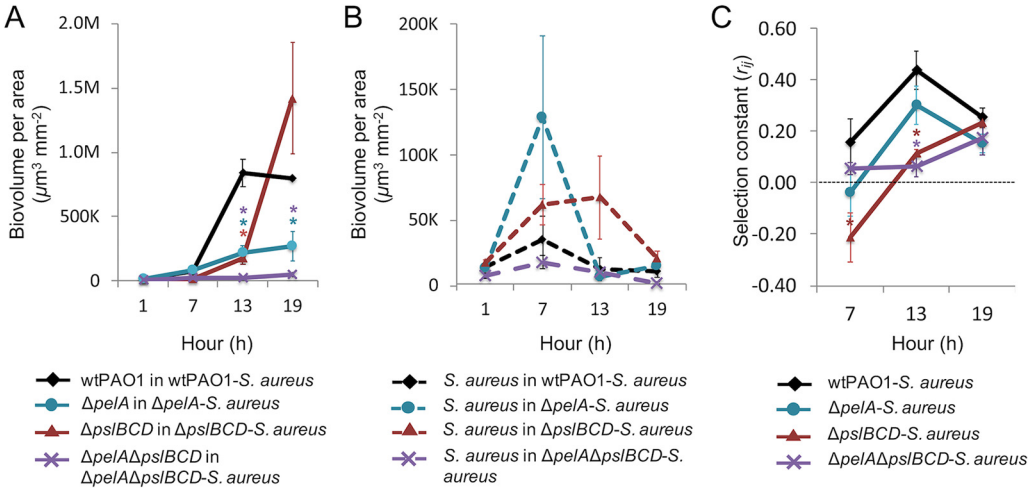

FIG 2 The development of 19-h biofilms formed by wild-type and matrix mutants of *P. aeruginosa* cocultured with *S. aureus*. Error bars represent standard errors of the means (SEM) ($n \geq 4$). *, $P < 0.05$, $\alpha = 0.05$ (unpaired two-sided *t* test with Welch's correction). (A) Biovolumes per area of *P. aeruginosa* (solid lines) in the dual-species biofilms every 6 h. (B) Biovolumes per area of *S. aureus* (dashed lines) in the dual-species biofilms every 6 h. Note that the *y* axis scales for panels A and B are different. (C) Fitness of *P. aeruginosa* relative to *S. aureus*, where a selection constant of $r_{ij} = 0$ means that *P. aeruginosa* and *S. aureus* are equally competitive and a r_{ij} value of >0 means *P. aeruginosa* is more competitive than *S. aureus*.

at 267,374 ± 114,530 μm³ mm^{-2} from 13 to 19 h. For the Δ*pslBCD* mutant, the average biovolume was unchanged at 7 h but was found to have increased by approximately 10-fold at 13 h and a further 10-fold by 19 h to achieve a final biovolume of 1,419,718 ± 432,200 μm³ mm^{-2}. For the Δ*pelA* Δ*pslBCD* mutant, the average biovolume increased in 3-fold increments at each 6-h time point to a final average biovolume of 50,401 ± 21,795 μm³ mm^{-2} at 19 h. Thus, the loss of Pel in the dual-species biofilms was associated with an overall reduction in total biovolume at 13 and 19 h (Fig. 2A).

The average biovolume of *S. aureus* for all biofilms increased initially but remained low throughout biofilm development compared to *P. aeruginosa* and by 19 h had returned to levels similar to or lower than those observed at the start of biofilm formation (Table 2) (Fig. 2B). There were no significant differences in the *S. aureus* biovolumes of the dual-species biofilms with different combinations of Pel and Psl expression.

The selection constant rates (r_{ij}), representing the ratios of *P. aeruginosa* over *S. aureus* over time, were derived from the biovolume data to determine the competitiveness of the *P. aeruginosa* wild-type and polysaccharide mutants against *S. aureus* (Table 3, columns 2 to 4). Only the Δ*pslBCD* mutant was less competitive than *S. aureus* after 7 h of biofilm formation (Table 3, columns 5 and 6) (Fig. 2C), and the r_{ij} value was significantly different from that determined for the wild-type ($P = 0.04$, $\alpha = 0.05$, $n =$

TABLE 3 Competitiveness of *P. aeruginosa* relative to *S. aureus*

Biofilm	Selection rate constant, r_{ij}[a]			Correlation of fitness curves[b]	
	7 h	13 h	19 h	Biofilm	r_{XY}
wtPAO1-*S. aureus*	0.16 ± 0.09	0.43 ± 0.07	0.25 ± 0.04	wtPAO1-*S. aureus* with Δ*pelA-S. aureus*	0.97
Mutant Δ*pelA-S. aureus*	−0.04 ± 0.20	0.30 ± 0.06	0.15 ± 0.04	wtPAO1-*S. aureus* with Δ*pslBCD-S. aureus*	0.58
Mutant Δ*pslBCD-S. aureus*	−0.21 ± 0.09*	0.12 ± 0.01*	0.23 ± 0.02	Δ*pelA-S. aureus* with Δ*pslBCD-S. aureus*	0.76
Mutant Δ*pelA* Δ*pslBCD-S. aureus*	0.06 ± 0.02	0.07 ± 0.04*	0.18 ± 0.07	wtPAO1-*S. aureus* with Δ*pelA* Δ*pslBCD-S. aureus*	-0.11
Mutant Δ*siaD-S. aureus*	0.11 ± 0.06	0.07 ± 0.04*	0.01 ± 0.01*	Δ*pelA-S. aureus* with Δ*pelA* Δ*pslBCD-S. aureus*	0.13
Mutant Δ*siaD*(*siaD*)-*S. aureus*	0.23 ± 0.05	0.19 ± 0.04	0.18 ± 0.05	Δ*pslBCD-S. aureus* with Δ*pelA* Δ*pslBCD-S. aureus*	0.75

[a]Data represent selection rate constants during 19 h of biofilm development determined from four biological replicates, with each replicate derived from an average of three confocal images. Asterisks (*) indicate a significant difference from the wild-type *P. aeruginosa-S. aureus* biofilms ($P < 0.05$) (unpaired *t* test with Welch's correction). Error data represent SEM.

[b]Correlation of fitness curves is given by the Pearson correlation coefficient (r_{XY}).

TABLE 4 Surface coverage, microcolony size, and number of microcolonies in single- and mixed-species biofilms[a]

Biofilm	Strain(s)	Avg surface coverage (%)		Avg no. of microcolony per area (mm^{-2})		Avg microcolony biovolume (μm^3)	
		13 h	19 h	13 h	19 h	13 h	19 h
Monospecies: *P. aeruginosa*	wtPAO1	14 ± 4	10 ± 2	1,757 ± 386	1,974 ± 360	109 ± 46	58 ± 23
Monospecies: *S. aureus* 15981	*S. aureus* 15981	20 ± 5	40 ± 10	2,520 ± 552	3,325 ± 507	1,346 ± 3,035	7,356 ± 2,279
Dual species: *P. aeruginosa*-*S. aureus*	wtPAO1 *S. aureus* 15981	19 ± 3 0 ± 2	22 ± 0 0 ± 0	5,265 ± 489	3,716 ± 462	108 ± 7	499 ± 91
Dual species: mutant Δ*pelA*-*S. aureus*	Mutant Δ*pelA* *S. aureus* 15981	8 ± 1 0 ± 0	9 ± 3 1 ± 0	1,025 ± 302	2,581 ± 1,117	67 ± 5	111 ± 19
Dual species: mutant Δ*pslBCD*-*S. aureus*	Mutant Δ*pslBCD* *S. aureus* 15981	7 ± 3 2 ± 1	33 ± 14 1 ± 0	1,043 ± 756 207 ± 138	4,661 ± 2,407 85 ± 85	50 ± 4 65 ± 16	1,400 ± 358 65 ± 15
Dual species: mutant Δ*pelA* Δ*pslBCD*-*S. aureus*	Mutant Δ*pelA* Δ*pslBCD* *S. aureus* 15981	3 ± 1 1 ± 0	5 ± 2 0 ± 0				

[a]Values are derived from three biological replicates, with each replicate derived from an average of three confocal images. Error data represent SEM.

4). At 13 h, the Δ*pslBCD* mutant was more competitive than *S. aureus* but the competitiveness was still lower than and significantly different from that seen with the wild-type ($P = 0.02$, $\alpha = 0.05$, $n = 4$). The Δ*pelA* Δ*pslBCD* mutant was significantly less competitive than the wild-type strain against *S. aureus* at 13 h ($P = 0.01$, $\alpha = 0.05$, $n = 4$) (Table 3, columns 2 to 4) (Fig. 2C). By 19 h, both the Δ*pslBCD* and Δ*pelA* Δ*pslBCD* mutants were as competitive as the wild-type strain against *S. aureus*.

Although the Δ*pelA* mutant was less competitive than the wild-type strain against *S. aureus* throughout biofilm formation, the differences were not statistically significant (Table 3, columns 2 to 4) (Fig. 2C). Based on the r_{ij} values, changes in the competitiveness of the Δ*pelA* mutant and wild-type *P. aeruginosa* were also similar for the dual-species biofilms, with r_{ij} reaching a peak at 13 h and the r_{ij} over time (fitness curves), displaying a strong positive correlation of $r_{XY} = 0.97$ (Table 3, columns 5 and 6) (Fig. 2C). Thus, Psl contributes to the competitive fitness of the wild-type strain only during the early stages of *P. aeruginosa*-*S. aureus* biofilm development.

***S. aureus* and Pel production are associated with an increase in surface coverage and in the microcolony size of *P. aeruginosa* in dual-species biofilms.** To explore how Pel and Psl affected the structure of dual-species biofilms (Fig. 1), the average surface coverage, the number of microcolonies, and the microcolony sizes of 13-h and 19-h biofilms were calculated (Table 4). Monospecies wild-type biofilms were also investigated for comparison to the dual-species, wild-type biofilms (Table 4). Microcolonies included small and large cell clusters, which ranged in size over various orders of magnitude (Fig. 3).

Wild-type *P. aeruginosa* displayed the highest surface coverage at 13 h compared to the matrix mutants in the dual-species biofilms. Wild-type *P. aeruginosa* had a surface coverage of 19% ± 3%, while the Δ*pelA* and Δ*pslBCD* mutants had similar surface coverages at 8% ± 1% and 7% ± 3%, respectively, and the Δ*pelA* Δ*pslBCD* mutant displayed a surface coverage of 3% ± 1% (Table 4). At 19 h, biofilms of wild-type *P. aeruginosa* and mutants Δ*pelA* and Δ*pelA* Δ*pslBCD* were similar to the 13-h biofilms at 22% ± 0%, 9% ± 3%, and 5% ± 2% surface coverage, respectively, whereas the Δ*pslBCD* mutant surface coverage increased to 33% ± 14% (Table 4). The surface coverage of *S. aureus* in the dual-species biofilms at 13 and 19 h ranged from 0% to 2% irrespective of whether wild-type or mutant *P. aeruginosa* was included (Table 4). *P. aeruginosa* had more surface coverage in dual-species biofilms than in monospecies biofilms at both 13 and 19 h. However, *S. aureus* had much less surface coverage at 13 and 19 h in cocultures with *P. aeruginosa* (Table 4).

Wild-type *P. aeruginosa* formed the greatest number of microcolonies compared to the mutants in the dual-species biofilms. The average microcolony size was 108 ± 7

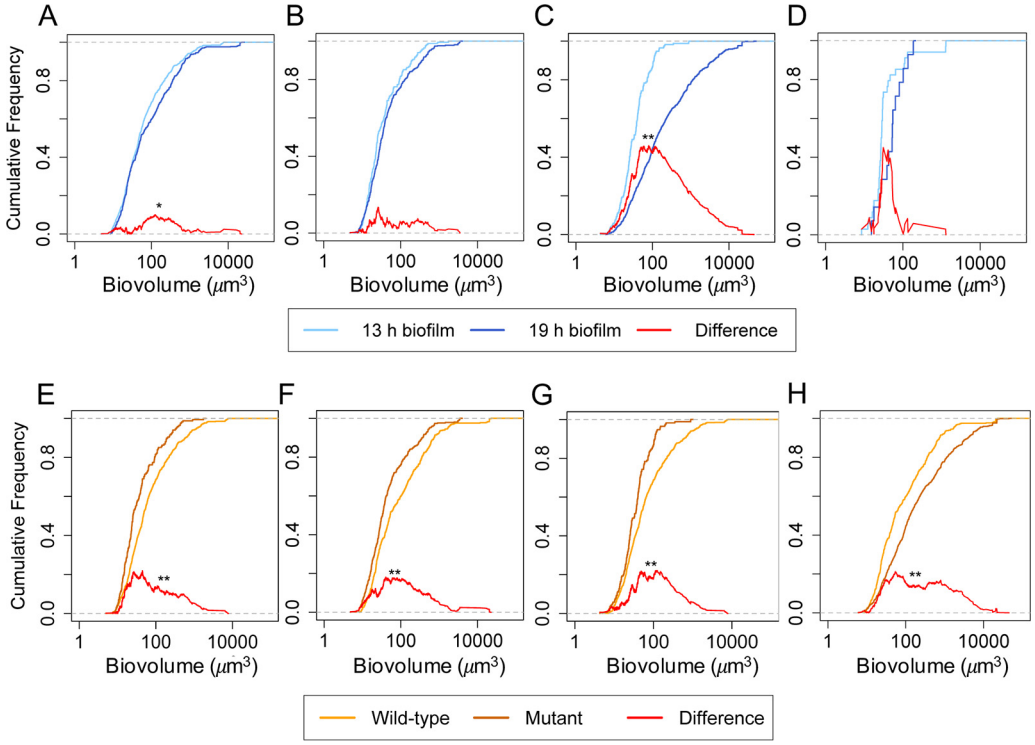

FIG 3 Comparison of microcolony sizes in dual-species biofilms using the two-sample, two-sided Kolmogorov-Smirnov test. The red curve shows the difference between the two distributions (*, $P < 0.05$, **, $P < 0.01$, ***, $P < 0.001$; $\alpha = 0.05$). (Top panel) Changes in size distribution as biofilms progresses from 13 to 19 h. (A to D) *P. aeruginosa* microcolonies in (A) wild-type *P. aeruginosa-S. aureus*, (B) mutant Δ*pelA-S. aureus*, and (C) mutant Δ*pslBCD-S. aureus* biofilms and *S. aureus* microcolonies in (D) mutant Δ*pslBCD-S. aureus* biofilms. (Bottom panel) Differences between *P. aeruginosa* microcolony size distributions formed by wild-type and matrix mutants of *P. aeruginosa* cocultured with *S. aureus*. (E and F) Wild-type *P. aeruginosa-S. aureus* compared to mutant Δ*pelA-S. aureus* at (E) 13 h and (F) 19 h. (G and H) Wild-type *P. aeruginosa-S. aureus* compared to mutant Δ*pslBCD-S. aureus* at (G) 13 h and (H) 19 h.

μm^3 at 13 h and increased to 499 ± 91 μm^3 by 19 h (Table 4) (Fig. 3A). Wild-type *P. aeruginosa* also formed more microcolonies as a dual-species biofilm than as a monospecies biofilm. The sizes of the microcolonies formed by *P. aeruginosa* in dual-species biofilms and monospecies biofilms were similar at 13 h, but the microcolonies in the dual-species biofilms were about 10 times larger than in the monospecies biofilms by 19 h.

The Δ*pelA* mutant formed approximately 5-fold-fewer microcolonies than the wild-type strain, and the average microcolony size was 67 ± 5 μm^3 at 13 h. By 19 h, the number of microcolonies had not increased, but the average microcolony size increased to 111 ± 19 μm^3 (Table 4). The microcolony size distributions were not significantly different as the biofilm progressed from 13 to 19 h (Fig. 3B). The Δ*pelA* microcolony size was significantly smaller than the wild-type microcolony size at both 13 h (Fig. 3E) and 19 h (Fig. 3F).

The Δ*pslBCD* mutant also formed approximately 5-fold-fewer microcolonies than the the wild-type strain by 13 h, and the average microcolony size was 50 ± 4 μm^3. By 19 h, the number of microcolonies had increased by ~5-fold and the average microcolony size had increased to 1,400 ± 358 μm^3 (Table 4). The microcolony size distribution at 19 h was larger than and significantly different from that seen of 13 h of biofilm development, with the difference between the two distributions being as large as 46% (Fig. 3C). The Δ*pslBCD* microcolony size distribution was smaller than that of the wild-type strain at 13 h (Fig. 3G) but was larger at 19 h (Fig. 3H).

The Δ*pelA* Δ*pslBCD* mutant did not form microcolonies in the dual-species biofilms. *S. aureus* also did not form microcolonies in any of the dual-species biofilms except when cultivated with the Δ*pslBCD* strain, with average microcolony sizes of 65 ± 16

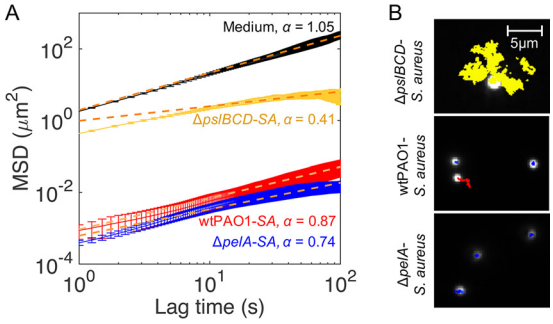

FIG 4 Microrheological measurements of wild-type and matrix mutants of *P. aeruginosa* cocultured with *S. aureus*. (A) MSD curves for wild-type *P. aeruginosa-S. aureus*, mutant Δ*pelA-S. aureus*, and mutant Δ*pslBCD-S. aureus* microcolonies. The MSD curve for TSB medium is shown for comparison. *SA*, *S. aureus*. The orange dotted lines indicate the line of best fit to the experimentally determined MSD using a power law function for the estimation of α. (B) Representative particle trajectories in wild-type *P. aeruginosa-S. aureus*, mutant Δ*pelA-S. aureus*, and mutant Δ*pslBCD-S. aureus* microcolonies. The red trajectory in the middle panel indicates a particle undergoing directed motion and superdiffusion, whereas the blue and yellow trajectories indicate subdiffusion. Error bars represent SEM.

μm^3 at 13 h and 65 $\pm$ 15 μm^3 by 19 h (Fig. 3D). Thus, expression of Psl was required for microcolony formation of *P. aeruginosa* and hindered *S. aureus* biofilm formation. Expression of Pel was required for expanding surface coverage and microcolonies.

Pel and Psl have opposing rheological roles in the matrix of the microcolonies. Biofilm rheological properties conferred by Pel and Psl affect biofilm structure and spreading at different stages in monospecies *P. aeruginosa* biofilms under flow conditions (33). Specifically, Psl cross-links the biofilm to increase microcolony formation and reduce spreading at the early stages, while Pel loosens the biofilm to increase spreading at the later stages of biofilm development (33). Thus, we investigated the rheological properties of 19-h dual-species biofilms using particle-tracking microrheology (37, 38) to determine if the mechanical roles of Pel and Psl in monospecies flow cell biofilms were maintained in *P. aeruginosa-S. aureus* static biofilms. If so, this could explain the increased surface coverage and microcolony sizes observed in *P. aeruginosa-S. aureus* biofilms expressing Pel.

The mean squared displacement (MSD) of particles embedded within microcolonies of 19-h biofilms was directly proportional to their creep compliance (J) and effective cross-linking (39, 40). The changes in effective cross-linking could have been due to differences in polymer chain length and concentration and degree of polymer entanglement and to interactions between different polymers. The interactions between polymers can be chemical (operating through covalent bonds), physical (operating through noncovalent interactions), or topological, depending on the polymeric entanglements. The MSDs were plotted as a function of lag time (elapsed time; 1 s $\leq t \leq$ 100 s) to give the MSD curves from which the power law exponent (α) can be derived. When $\alpha = 1$, the particle is considered to be undergoing normal diffusion; when $\alpha < 1$, this is termed subdiffusion; and when $\alpha > 1$, they are considered to be undergoing superdiffusion (41, 42). The diffusive regime also informs one of the rheological environment in which the particle is embedded. For example, when $\alpha = 0$, the substance is purely elastic; when $0 < \alpha < 1$, the substance is viscoelastic; and when $\alpha = 1$, the substance is purely viscous (37, 38). The undifferentiated layers in wild-type *P. aeruginosa-S. aureus* and mutant Δ*pelA-S. aureus* that trapped the particles were too thin for investigation without an attachment to or a capillary effect from the substratum and hence were not investigated. The rheological parameters of the sterile TSB medium (17 g liter^{-1} casein peptone, 2.5 g liter^{-1} K_2HPO_4, 2.5 g liter^{-1} glucose, 5 g liter^{-1} NaCl, 3 g liter^{-1} soya peptone) were characteristic of a viscous Newtonian fluid at $\alpha = 1.04$ and $J = 11{,}500 \pm 789$ Pa^{-1} at $t = 10^1$ s (Fig. 4A) (Table 5). In comparison, the wild-type *P. aeruginosa-S. aureus* microcolonies displayed creep compliance of $J = 3 \pm 2$ Pa^{-1} at $t = 10^1$ s and a power law exponent α value of 0.87 (Fig. 4A). In addition, several

TABLE 5 Viscoelasticity and creep compliance of 19-h biofilms formed by *P. aeruginosa* and matrix polysaccharide mutants with *S. aureus*, respectively

Biofilm	Region	α	$J(t)$ (t = 101 s, Pa^{-1})
Medium (negative control)	Liquid phase	1.05	11,500 ± 789
wtPAO1-*S. aureus*	Microcolony	0.87	3 ± 2
Mutant Δ*pelA*-*S. aureus*	Microcolony	0.74	2 ± 0
Mutant Δ*pslBCD*-*S. aureus*	Loose microcolony	0.41	1,294 ± 109

particles were observed to undergo superdiffusion, which was also defined by their directional movement, with a net displacement of 1 to 3 μm within a 15-min period, compared to particle vibrations, with a net displacement of <1 μm (Fig. 4B) and α = 1.59 (see Fig. S1 in the supplemental material).

The Δ*pelA*-*S. aureus* microcolonies had lower particle MSDs and thus were more effectively cross-linked than wild-type *P. aeruginosa*-*S. aureus* biofilm microcolonies (Fig. 4A). None of the particles were observed to undergo superdiffusion (Fig. 4B). The microcolonies had a creep compliance $J = 2 \pm 0\ Pa^{-1}$ at $t = 10^1$ s and were more elastic (α = 0.74) (Table 5).

Particles in mutant Δ*pslBCD*-*S. aureus* microcolonies were less confined, indicating a reduction in cross-linking (Fig. 4B). Mutant Δ*pslBCD*-*S. aureus* biofilms had creep compliance of 1,294 ± 109 Pa^{-1} and were more elastic (α = 0.41) (Table 5). The viscoelastic properties of the microcolonies formed in the dual-species *P. aeruginosa*-*S. aureus* and mutant Δ*pelA*-*S. aureus* biofilms in this study were different from those seen with the monospecies *P. aeruginosa* biofilms cultivated under flow conditions, as previously reported (33), where the microcolonies were elastic. However, the cross-linking role of Psl and matrix loosening mediated by Pel in monospecies biofilms were maintained in the *P. aeruginosa*-*S. aureus* community, regardless of flow conditions. The reduced matrix stiffness conferred by Pel may have contributed to the superdiffusive microenvironment for enabling microcolony expansion and increased surface coverage.

The competitive fitness of *P. aeruginosa* requires DGC SiaD. According to the selection constant rates (r_{ij}), changes in the extent of competitiveness of the Δ*pelA* mutant over *S. aureus* were similar to those seen with wild-type *P. aeruginosa* during dual-species biofilm development, whereas Δ*pslBCD* and Δ*pelA* Δ*pslBCD* mutants were less competitive in early biofilms (Fig. 2B) (Table 3, columns 5 and 6). This suggests that Psl is important for the competitive fitness of *P. aeruginosa* during early biofilm development. Psl has an active signaling role in biofilm formation, where it stimulates the activity of two DGCs, SiaD and SadC, thereby elevating intracellular c-di-GMP content (31, 32). This mechanism may also facilitate the competitiveness of *P. aeruginosa* in the *P. aeruginosa*-*S. aureus* community (31, 32). Indeed, Δ*pslBCD* mutants are delayed in biofilm development (25), which may have allowed *S. aureus* to form microcolonies in the dual-species biofilm.

P. aeruginosa competitiveness may also be associated with other molecules that interact with Psl. CdrA is a *P. aeruginosa* adhesin that binds to Psl and cross-links Psl polysaccharide polymers to increase the structural stability of the biofilm (28). We thus examined the effects of SiaD and SadC as well as of CdrA on *P. aeruginosa* competitiveness. The Δ*cdrA* and Δ*sadC* mutants dominated the dual-species biofilms, indicating that CdrA and SadC were not essential for *P. aeruginosa* competitiveness (Fig. 5A and B). Their fitness curves are given in Fig. S2. The biofilms were largely flat and undifferentiated, with small microcolonies (Fig. 5B). The loss of the SiaD DGC resulted in a significant reduction in competitive fitness for *P. aeruginosa* in mutant Δ*siaD*-*S. aureus* biofilms, with $r_{ij} = 0.07 \pm 0.04$ at 12 h and $r_{ij} = 0.01 \pm 0.01$ at 19 h, which were different from the results seen with the wild-type strain ($P < 0.01$, α = 0.05, n = 4) (Table 3, columns 2 to 4) (Fig. S2). There was little colocalization of *P. aeruginosa* and *S. aureus* in the biofilms, and *S. aureus* formed homogenous microcolonies devoid of *P. aeruginosa* Δ*siaD* cells (Fig. 5C). The rheological properties of these microcolonies, with monospecies *S. aureus* microcolonies investigated for comparison, are shown in

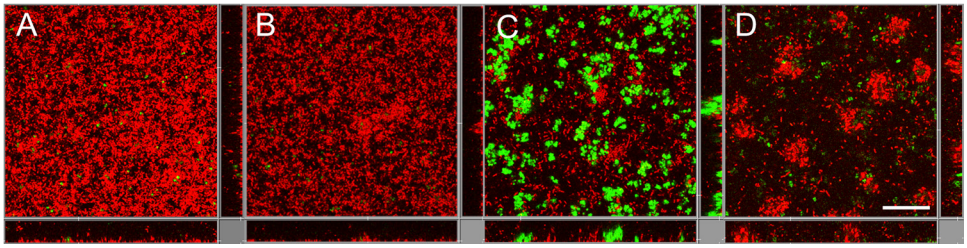

FIG 5 Confocal images of 19-h biofilms of *P. aeruginosa* CdrA and diguanylate cyclase mutants cocultured with *S. aureus*. (A) *P. aeruginosa* Δ*cdrA-S. aureus*. (B) *P. aeruginosa* Δ*sadC-S. aureus*. (C) *P. aeruginosa* Δ*siaD-S. aureus*. (D) *P. aeruginosa* Δ*siaD*(*siaD*)*-S. aureus*. *P. aeruginosa* was mCherry tagged (red), and *S. aureus* was Gfp tagged (green). Images are representative of results from at least three biological replicates. The scale bar is 30 μm.

Table S1 and Fig. S3 in the supplemental material. Genetic complementation of the Δ*siaD* mutant restored *P. aeruginosa* competitiveness ($r_{ij} = 0.18 \pm 0.05$), and the formation of microcolonies was dominated by *P. aeruginosa* after 19 h (Table 3, columns 2 to 4) (Fig. 5D). *P. aeruginosa* dominated regions of mutant Δ*cdrA-S. aureus*, mutant Δ*sadC-S. aureus* and mutant Δ*siaD-S. aureus* biofilms (Fig. 5) and had higher particle MSDs than the wild-type strain but less than the mutant Δ*pslBCD-S. aureus* microcolonies (Fig. 6). Thus, Psl remained the major contributor of matrix cross-linking although CdrA and c-di-GMP, though the SadC and SiaD signaling pathway also contributed to matrix cross-linking and biofilm stability. Further details of the number and size of microcolonies and of the rheological properties of the biofilm structures are given in Table S1.

SiaD-mediated competition is siderophore and PQS independent. *P. aeruginosa* uses the iron siderophore pyoverdine and products of *pqs* genes, such as N-oxo-2-heptyl-4-hydroxyquinoline (HQNO), to outcompete *S. aureus* in cocultures (18, 43). Hence, we examined whether the *P. aeruginosa* SiaD-mediated competition with *S. aureus* involved pyoverdine and PQS expression. The pyoverdine levels of the dual-species biofilms were estimated by measuring fluorescence at 450 nm, the peak level of emission for pyoverdine (44). The PQS levels were determined based on Gfp fluorescence using a PQS biosensor strain, Δ*pqsC*(*pqsA-gfp*), where the Δ*pqsC* mutant is unable to synthesize its own PQS and *pqsA-gfp* can only be induced by exogenously added PQS (45). Using these approaches, we found that the levels of production of pyoverdine (Fig. 7A) and PQS (Fig. 7B) of wild-type *P. aeruginosa* and the SiaD mutant were similar and that complementation of SiaD resulted in pyoverdine and PQS levels lower than those measured for the wild type. These results suggest that the inability of the SiaD mutant to compete with *S. aureus* was not due to a deficiency of pyoverdine and PQS production.

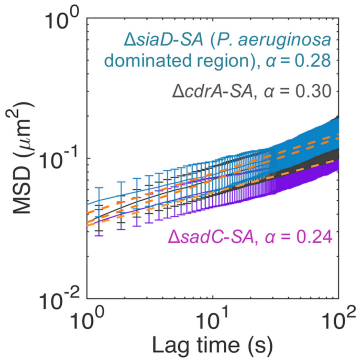

FIG 6 MSD curves for *P. aeruginosa* Δ*siaD-S. aureus*, *P. aeruginosa* Δ*cdrA-S. aureus*, and *P. aeruginosa* Δ*sadC-S. aureus* microcolonies. *SA*, *S. aureus*. The orange dotted lines indicate the line of best fit to the experimentally determined MSD using a power law function for the estimation of α. Error bars represent SEM.

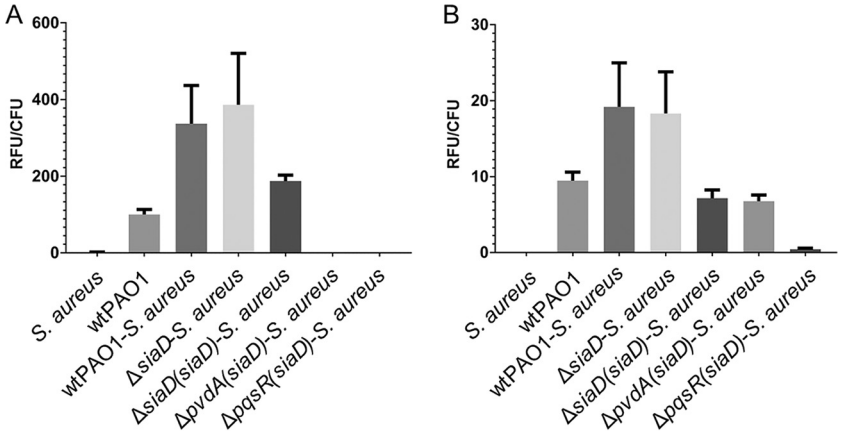

FIG 7 Relative levels of pyoverdine and PQS in 19-h *P. aeruginosa-S. aureus* biofilms. (A) Pyoverdine, as indicated by its fluorescence at an emission peak of 450 nm. (B). PQS, as indicated by the fluorescence emission of the green fluorescent protein from the PQS biosensor strain, mutant Δ*pqsC*(*pqsA-gfp*). Values are means (± standard deviations [SD]) of relative fluorescence units (RFU) determined from three biological replicates.

DISCUSSION

Coinfections of *P. aeruginosa* and *S. aureus* are often found in patients with cystic fibrosis (CF) and with diabetic and chronic wounds. Such mixed-species infections are correlated with poor clinical outcomes (16); hence, these two organisms serve as a model, dual-species community to represent polymicrobial infections (18, 43, 46). The interactions between the two organisms affect the efficacy of antimicrobial treatments (46). *P. aeruginosa* has been found to compete with *S. aureus* for oxygen and to induce the bacterium to shift to fermentative metabolism to produce lactate, which *P. aeruginosa* consumes (18). *P. aeruginosa* can also lyse *S. aureus* to obtain iron. This is mediated through induction of PQS-dependent virulence genes as well as the production of siderophores (43). However, detailed investigation of interspecies interactions during dual-species biofilm formation and the role of the biofilm matrix in enabling interspecies interactions and determining community structure have been less extensively explored.

In this study, *P. aeruginosa* restricted *S. aureus* growth and biofilm formation, whereas in the presence of *S. aureus*, *P. aeruginosa* showed an increased surface coverage and number of microcolonies. Further, *P. aeruginosa* microcolonies were larger and the overall biovolume was higher when *S. aureus* was present. Similar observations were previously reported for these dual-species combinations, where it was suggested that *P. aeruginosa* lysed *S. aureus* to be used as a nutrient source (18, 43). Pel and Psl polysaccharides were not required for *P. aeruginosa* to outcompete *S. aureus*, which was similar to the result seen with mucoid *P. aeruginosa-S. aureus* biofilms (33). Nevertheless, distinct effects contributed by the polysaccharides, such as reduced formation of *S. aureus* microcolonies during early biofilm development (mediated by Psl) and increased biofilm biovolumes of *P. aeruginosa* during mid- to late-stage biofilm development by Pel, were observed. These findings are consistent with a shift in production with time of biofilm formation, from Psl to Pel, similar to that documented for monospecies biofilms (33). In addition, the data indicate that Pel increases surface coverage throughout biofilm development and expands the microcolony size in mature biofilms. This finding aligns with that of our previous study, i.e., that Pel enhances spreading in monospecies biofilms (33). The latter study also attributed the differences in biofilm structures to Psl generating a more elastic and cross-linked matrix and Pel contributing a loose and viscoelastic matrix. Indeed, in agreement with the results obtained for monospecies biofilms, we found that Psl increased the effective cross-linking of the microcolonies in dual-species biofilms (Fig. 4), making them less compliant (Table 5) and more compact (Fig. 1). Psl was the major contributor of effective

cross-linking in the biofilm, while the CdrA adhesin and biofilm regulatory components SadC and SiaD played less of a role (Fig. 6) (see also Table S1 in the supplemental material).

Interestingly, the microcolonies that expressed only Pel were more elastic than the microcolonies that expressed only Psl, and the microcolonies that expressed both Pel and Psl were the most viscous. This indicated that the rheological contributions of the polysaccharides were not simply additive and that the physical structure changed in the absence of one of these polysaccharides. In addition to changes in the mechanical properties of the biofilm in the presence of *S. aureus*, it is possible that the Psl matrix is more viscous when it is produced under static versus flow conditions. This may reflect observations of biofilms on rocks beneath waterfalls that are constantly exposed to high shear (47, 48). The expression levels of both Pel and Psl were associated with superdiffusion of particles and with a more compliant biofilm matrix (Fig. 4) (Table 5). The superdiffusion of particles could be the result of fast movement of cells. *P. aeruginosa* is known to be motile, mediated by swimming, swarming, and twitching based processes. Superdiffusion could also be the result of particles travelling directionally through biofilm channels. For example, Birjiniuk et al. (2014) observed particle trajectories that indicated that the particles were travelling from top to the bottom of the biofilm through interconnected fluid-filled microscale channels (49).

The ability of Psl to initiate *P. aeruginosa* biofilm formation and mediate competitive fitness may be linked to its ability to facilitate biofilm formation through activating DGCs, leading to c-di-GMP production. Indeed, the SiaD DGC, activated by Psl (31), was critical for *P. aeruginosa* competitiveness in the dual-species biofilms (Fig. 5). Without SiaD, *P. aeruginosa* and *S. aureus* were equally competitive, with $r_{ij} = 0.01 \pm 0.04$ at 19 h, with *S. aureus* establishing many microcolonies in the dual-species biofilm (Fig. 5). Moreover, SiaD induces autoaggregation in *P. aeruginosa* when exposed to SDS stress (50) and /tellurite (TeO_3^{2-}) (32). In a previous study (50), Psl was found to be essential for autoaggregation. Hence, it is possible that SiaD is activated by exoproducts from *S. aureus*, providing a mechanism by which *P. aeruginosa* can sense *S. aureus* to induce autoaggregation and biofilm formation.

P. aeruginosa is known to outcompete *S. aureus* using the siderophore pyoverdine and downstream products of the PQS biosynthetic pathway in planktonic cultures (18, 43). In monospecies *P. aeruginosa* biofilms, SiaD has been found to negatively control pyoverdine production (51). Similarly, high c-di-GMP concentrations reduce PQS production (52). Thus, it was unexpected that the production levels of pyoverdine and PQS in the Δ*siaD* mutant were not increased but rather were similar to those seen with wild-type *P. aeruginosa* biofilm cocultures (Fig. 7). Complementation of the *siaD* mutant resulted in pyoverdine and PQS levels similar to the levels seen with wild-type *P. aeruginosa* monospecies biofilms but not dual-species wild-type biofilms (Fig. 7). This indicated that the overproduction of PQS in the *siaD* mutant does not play a significant role in the competitive phenotype here and that the impact of overproducing SiaD and, hence, of elevated c-di-GMP levels drives competition through another factor that is siderophore and PQS independent. Further investigation is required to understand the underlying mechanism of how SiaD activity increases the competitiveness of *P. aeruginosa*.

The findings presented here provide novel information on the mechanisms by which the *P. aeruginosa-S. aureus* dual-species biofilms are established and how *P. aeruginosa* dominates the community during biofilm development. We summarize the findings in Fig. 8, where we show that the Psl polysaccharide is required for initial competition whereas the Pel polysaccharide enables the predominance of *P. aeruginosa* in mature, dual-species biofilms (Fig. 8A). It is also clear that the SiaD cyclase is important for *P. aeruginosa* competitiveness, which occurs in a pyoverdine- and PQS-independent fashion, with the *siaD* mutant producing amounts similar to those produced by the wild-type strain and the complemented *siaD* mutant producing less than the wild-type, dual-species biofilms (Fig. 8B). This highlights the fact that the regulatory mechanisms governing competition between *P. aeruginosa* and *S. aureus* are likely to

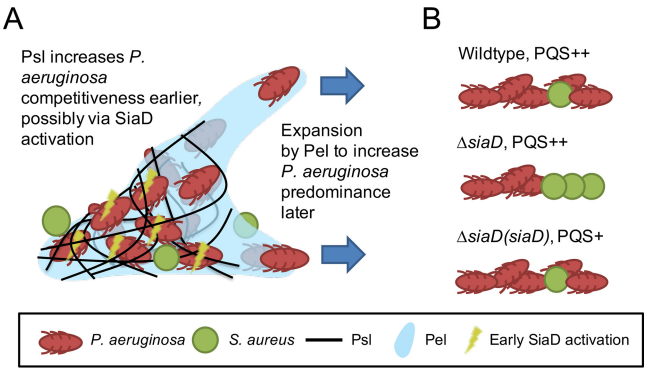

FIG 8 Schematic showing how matrix polysaccharides and SiaD contribute to *P. aeruginosa* predominance in dual-species *P. aeruginosa*-*S. aureus* communities. (A) Psl enhances *P. aeruginosa* competitiveness in early stages, possibly via SiaD activation, whereas Pel enables biofim expansion to increase *P. aeruginosa* predominance in the later stages. (B) Dominance of wild-type *P. aeruginosa* and SiaD and SiaD complement mutant over *S. aureus*, with their corresponding PQS/pyoverdine (PVD) levels.

be complex, incorporating recognition of a competitor and temporal regulation of different factors that impact the dual-species interactions. These results help to increase understanding of the mechanisms by which these two opportunistic pathogens interact during biofilm formation and could suggest strategies for the control of dual-species infections.

MATERIALS AND METHODS

Bacterial strains. The bacterial strains and plasmids used in this study are listed in Table 1. Overnight cultures of *P. aeruginosa* were grown in 100% LB medium (10 g liter^{-1} NaCl, 5 g liter^{-1} yeast extract, and 10 g liter^{-1} tryptone) at 37°C with shaking (200 rpm). *S. aureus* was grown in 100% TSB medium (17 g liter^{-1} casein peptone, 2.5 g liter^{-1} K_2HPO_4, 2.5 g liter^{-1} glucose, 5 g liter^{-1} NaCl, 3 g liter^{-1} soya peptone) at 37°C with shaking (200 rpm).

Construction of *Pseudomonas aeruginosa* mutants. The Δ*sadC* and Δ*siaD* mutants, defective in production of SadC and SiaD diguanylate cyclases, respectively, were constructed by homologous recombination as previously described (51, 53). The Δ*cdrA* mutant, defective for the CdrA adhesin, was constructed by homologous recombination using lambda Red recombinase as previously described (54) with a Multisite Gateway (Thermo Fisher Scientific, MA) LR expression clone containing the PCR product 5′ CdrA upstream fragment, gentamicin gene, 3′ CdrA downstream fragment (primers 5′ CdrA upstream F [GGGG ACA ACT TTG TAT AGA AAA GTT G AGGGTCTTGCCTTCCAGTTC] and R [GGGG AC TGC TTT TTT GTA CAA ACT TG GAAAATCTCCCTATCTGCGTGG] and 3′ CdrA downstream F [GGGG ACA GCT TTC TTG TAC AAA GTG G TCCTCGAAAACCCGTTCCTG] and R [GGGG AC AAC TTT GTA TAA TAA AGT TG CTTCGT ATCGCTGCTGTTGC]). A pUCP18-*siaD* plasmid (51) was used to genetically complement the *P. aeruginosa* Δ*siaD* mutant.

Cultivation of static biofilms. Overnight cultures of *P. aeruginosa* and *S. aureus* were diluted with TSB medium to optical densities at 600 nm (OD_{600}) of 0.01 and 0.02, respectively, to yield cell densities of approximately 2 × 10^7 CFU ml^{-1}. For monospecies biofilm cultivation, μ-Side eight-well microscopy chambers (ibidi, Martinsried, Germany) were inoculated with 200 μl of diluted overnight cultures of *P. aeruginosa* or *S. aureus*. For dual-species biofilms, μ-Slide eight-well microscopy chambers were inoculated with 100 μl of *P. aeruginosa* and *S. aureus* each to give total initial cell densities similar to those of the monospecies biofilms with 1:1 ratios. The cultures were incubated at 37°C under static conditions.

Biofilm image acquisition and analysis. Biofilms were visualized using a Zeiss LSM780 confocal scanning laser microscopy (Oberkochen). *P. aeruginosa* strains were fluorescently marked using miniTn7-mCherry (55). mCherry was detected using an argon laser for excitation at a wavelength of 568 nm and a low-pass emission filter at a wavelength of 590 nm. *S. aureus* 15981 was fluorescently marked using pSB2019, expressing Gfp (56). Gfp was detected using an argon laser for excitation at a wavelength of 488 nm and a broad-pass emission filter at wavelengths of 500 to 530 nm. Images were reconstructed using the Imaris software package (Bitplane, AG), and the biovolumes, microcolony numbers and sizes, and surface coverage values were calculated using COMSTAT (www.comstat.dk; see Table S1 in the supplemental material) (57, 58). Biovolumes were measured and calculated from four biological replicates, whereas microcolony sizes and surface coverages were calculated from three biological replicates. Each biological replicate was derived from an average of three confocal images. The mean and variance of microcolony sizes were derived after logarithmic transformation of the data according to their lognormal distribution (59). Significant differences between the distributions of microcolony sizes were determined by the Kolmogorov-Smirnov test. The competitiveness of bacterial species *i* over *j* was expressed as the selection rate constant (r_{ij}), which was calculated according to the equation r_{ij} =

$\frac{\ln\left(\frac{N_i(t)}{N_i(0)}\right)-\ln\left(\frac{N_j(t)}{N_j(0)}\right)}{t}$, where t is time in hours and N is the biovolume of species i or j at the start ($t = 0$) or at time t (60). The competitiveness levels of the two different species are equal when $r_{ij} = 0$.

Microrheology. Fluorescent latex beads 1.0 μm in diameter and with carboxylate modification (Invitrogen, CA) were dispersed in TSB medium to reach a final concentrations of 18.2×10^6 particles ml^{-1}, and medium was used to dilute the overnight cultures and to grow biofilms. After particle incorporation into the biofilms, their movement was tracked by fluorescence microscopy with a 63× objective (Zeiss Axio Observer Z1). The motion of particles in the cocultures was captured in 15-min videos at frame rates of 1 to 5 fps. The particle trajectories were obtained with ImageJ (https://fiji.sc/) (61) plugin Mosaic Particle Tracker (62). The trajectories were pooled for each biofilm, and the mean squared displacement (MSD) values were calculated and analyzed using msdanalyzer (63), a MATLAB class for MSD analysis. The MSD is proportional to the creep compliance, $J(t)$, of the material according to the following relation:

$$J(t) = \frac{3\pi d}{4k_B T}\mathrm{MSD}(t)$$

where J = creep compliance, d = particle diameter, k_B = Boltzman constant, and T = temperature (37, 39). The microrheological properties are related to the MSD levels, which in our work here are well described by MSD (t) ~ t^{α} (37, 38, 41). The values of α were extracted from the logarithmic fit to the MSD for a lag time range of approximately 1 s to 100 s. The R^2 values of the curves were greater than 0.96.

Pyoverdine and Pseudomonas quinolone signal (PQS) assay. Monospecies and dual-species biofilms were grown in 24-well plates for 19 h (Nunc 142475 Nunclon). The wells were centrifuged at 13,000 × *g* for 3 min to separate and obtain cell pellets and supernatants. The cell pellets were resuspended and plated onto Pseudomonas isolation agar for CFU counting of *P. aeruginosa* cells. Cells from monospecies *S. aureus* biofilms were plated on TSB agar for CFU counting. The supernatants filtered with 0.2-μm-pore-size Acrodisc PF syringe filters with Supor membrane (Pall Life Sciences, USA). For the pyoverdine assay, the relative levels of pyoverdine in the supernatants were estimated from their emission fluorescence at 450 nm using laser excitation at 400 nm with a Magellan Tecan Infinite 200 Pro microplate reader (Männedorf). For the PQS assay, 100 μl of 50× diluted overnight cultures of PQS biosensor strain Δ*pqsC*(*pqsA-gfp*) was mixed with 100 μl of the filtered biofilm supernatants. The mixtures were then cultivated in a 96-well microplate at 37°C. Green fluorescent protein (GFP) fluorescence from *pqsA-gfp* expression was measured using a Magellan Tecan Infinite 200 Pro microplate reader (Männedorf) to indicate PQS levels. All emission fluorescence readings were normalized to the CFU of *P. aeruginosa*.

SUPPLEMENTAL MATERIAL

Supplemental material for this article may be found at https://doi.org/10.1128/mBio.00585-18.

TEXT S1, DOCX file, 0.01 MB.

FIG S1, PDF file, 0.2 MB.

FIG S2, PDF file, 0.01 MB.

FIG S3, PDF file, 0.1 MB.

TABLE S1, DOCX file, 0.01 MB.

ACKNOWLEDGMENTS

We thank Seow Fong Chin for her help in molecular cloning of *P. aeruginosa*.

This research was supported by the National Research Foundation and Ministry of Education Singapore under its Research Centre of Excellence Program and AcRF Tier 2 (MOE2014-T2-2-172) from Ministry of Education, Singapore. We acknowledge the Singapore-MIT Alliance for Research and Technology Centre, which participates in the National Research Foundation program at CREATE. S.C.C. was further supported by the SMART Scholar Fellowship and J.K. by an individual research grant from the German Science Foundation (DFG; KL 2340/2-1).

The work presented here was carried out in collaboration between all authors. L.Y., S.C.C., S.K., and S.A.R. defined the research theme. S.C.C., J.K.H.Y., A.M., J.K., and L.Y. designed methods and experiments, carried out the laboratory experiments, analyzed the data, and interpreted the results. Z.J.S. constructed exopolysaccharide (EPS) mutants of *P. aeruginosa*. S.C.C., J.K., S.A.R., M.G., L.Y., and S.K. discussed analyses, interpretation, and presentation and wrote the paper. All of us contributed to, saw, and approved the manuscript.

REFERENCES

1. Costerton JW, Lewandowski Z, Caldwell DE, Korber DR, Lappin-Scott HM. 1995. Microbial biofilms. Annu Rev Microbiol 49:711–745. https://doi.org/10.1146/annurev.mi.49.100195.003431.
2. Costerton JW, Stewart PS, Greenberg EP. 1999. Bacterial biofilms: a common cause of persistent infections. Science 284:1318–1322. https://doi.org/10.1126/science.284.5418.1318.
3. Peter H, Ylla I, Gudasz C, Romani AM, Sabater S, Tranvik LJ. 2011. Multifunctionality and diversity in bacterial biofilms. PLoS One 6:e23225. https://doi.org/10.1371/journal.pone.0023225.
4. Cao B, Majors PD, Ahmed B, Renslow RS, Silvia CP, Shi L, Kjelleberg S, Fredrickson JK, Beyenal H. 2012. Biofilm shows spatially stratified metabolic responses to contaminant exposure. Environ Microbiol 14:2901–2910. https://doi.org/10.1111/j.1462-2920.2012.02850.x.
5. Moller S, Sternberg C, Andersen JB, Christensen BB, Ramos JL, Givskov M, Molin S. 1998. *In situ* gene expression in mixed-culture biofilms: evidence of metabolic interactions between community members. Appl Environ Microbiol 64:721–732.
6. Mah TFC, O'Toole GA. 2001. Mechanisms of biofilm resistance to antimicrobial agents. Trends Microbiol 9:34–39. https://doi.org/10.1016/S0966-842X(00)01913-2.
7. Burmolle M, Webb JS, Rao D, Hansen LH, Sorensen SJ, Kjelleberg S. 2006. Enhanced biofilm formation and increased resistance to antimicrobial agents and bacterial invasion are caused by synergistic interactions in multispecies biofilms. Appl Environ Microbiol 72:3916–3923. https://doi.org/10.1128/AEM.03022-05.
8. Leid JG, Willson CJ, Shirtliff ME, Hassett DJ, Parsek MR, Jeffers AK. 2005. The exopolysaccharide alginate protects *Pseudomonas aeruginosa* biofilm bacteria from IFN-gamma-mediated macrophage killing. J Immunol 175:7512–7518. https://doi.org/10.4049/jimmunol.175.11.7512.
9. Cotter PA, Stibitz S. 2007. c-di-GMP-mediated regulation of virulence and biofilm formation. Curr Opin Microbiol 10:17–23. https://doi.org/10.1016/j.mib.2006.12.006.
10. DiGiovanni GD, Neilson JW, Pepper IL, Sinclair NA. 1996. Gene transfer of *Alcaligenes eutrophus* JMP134 plasmid pJP4 to indigenous soil recipients. Appl Environ Microbiol 62:2521–2526.
11. Ghigo JM. 2001. Natural conjugative plasmids induce bacterial biofilm development. Nature 412:442–445. https://doi.org/10.1038/35086581.
12. Davey ME, O'toole GA. 2000. Microbial biofilms: from ecology to molecular genetics. Microbiol Mol Biol Rev 64:847–867. https://doi.org/10.1128/MMBR.64.4.847-867.2000.
13. Beech IB, Sunner J. 2004. Biocorrosion: towards understanding interactions between biofilms and metals. Curr Opin Biotechnol 15:181–186. https://doi.org/10.1016/j.copbio.2004.05.001.
14. Hall-Stoodley L, Costerton JW, Stoodley P. 2004. Bacterial biofilms: from the natural environment to infectious diseases. Nat Rev Microbiol 2:95–108. https://doi.org/10.1038/nrmicro821.
15. Willner D, Haynes MR, Furlan M, Schmieder R, Lim YW, Rainey PB, Rohwer F, Conrad D. 2012. Spatial distribution of microbial communities in the cystic fibrosis lung. ISME J 6:471–474. https://doi.org/10.1038/ismej.2011.104.
16. Limoli DH, Yang J, Khansaheb MK, Helfman B, Peng L, Stecenko AA, Goldberg JB. 2016. *Staphylococcus aureus* and *Pseudomonas aeruginosa* co-infection is associated with cystic fibrosis-related diabetes and poor clinical outcomes. Eur J Clin Microbiol Infect Dis 35:947–953. https://doi.org/10.1007/s10096-016-2621-0.
17. Yang L, Liu Y, Markussen T, Hoiby N, Tolker-Nielsen T, Molin S. 2011. Pattern differentiation in co-culture biofilms formed by *Staphylococcus aureus* and *Pseudomonas aeruginosa*. FEMS Immunol Med Microbiol 62:339–347. https://doi.org/10.1111/j.1574-695X.2011.00820.x.
18. Filkins LM, Graber JA, Olson DG, Dolben EL, Lynd LR, Bhuju S, O'Toole GA. 2015. Coculture of *Staphylococcus aureus* with *Pseudomonas aeruginosa* drives *S. aureus* towards fermentative metabolism and reduced viability in a cystic fibrosis model. J Bacteriol 197:2252–2264. https://doi.org/10.1128/JB.00059-15.
19. Machan ZA, Taylor GW, Pitt TL, Cole PJ, Wilson R. 1992. 2-Heptyl-4-hydroxyquinoline N-oxide, an antistaphylococcal agent produced by *Pseudomonas aeruginosa*. J Antimicrob Chemother 30:615–623. https://doi.org/10.1093/jac/30.5.615.
20. Biswas L, Biswas R, Schlag M, Bertram R, Gotz F. 2009. Small-colony variant selection as a survival strategy for *Staphylococcus aureus* in the presence of *Pseudomonas aeruginosa*. Appl Environ Microbiol 75:6910–6912. https://doi.org/10.1128/AEM.01211-09.
21. Pernet E, Guillemot L, Burgel PR, Martin C, Lambeau G, Sermet-Gaudelus I, Sands D, Leduc D, Morand PC, Jeammet L, Chignard M, Wu Y, Touqui L. 2014. *Pseudomonas aeruginosa* eradicates *Staphylococcus aureus* by manipulating the host immunity. Nat Commun 5:5105. https://doi.org/10.1038/ncomms6105.
22. Franklin MJ, Nivens DE, Weadge JT, Howell PL. 2011. Biosynthesis of the *Pseudomonas aeruginosa* extracellular polysaccharides, alginate, Pel, and Psl. Front Microbiol 2:167. https://doi.org/10.3389/fmicb.2011.00167.
23. Wozniak DJ, Wyckoff TJO, Starkey M, Keyser R, Azadi P, O'Toole GA, Parsek MR. 2003. Alginate is not a significant component of the extracellular polysaccharide matrix of PA14 and PAO1 *Pseudomonas aeruginosa* biofilms. Proc Natl Acad Sci U S A 100:7907–7912. https://doi.org/10.1073/pnas.1231792100.
24. Friedman L, Kolter R. 2004. Two genetic loci produce distinct carbohydrate-rich structural components of the *Pseudomonas aeruginosa* biofilm matrix. J Bacteriol 186:4457–4465. https://doi.org/10.1128/JB.186.14.4457-4465.2004.
25. Colvin KM, Irie Y, Tart CS, Urbano R, Whitney JC, Ryder C, Howell PL, Wozniak DJ, Parsek MR. 2012. The Pel and Psl polysaccharides provide *Pseudomonas aeruginosa* structural redundancy within the biofilm matrix. Environ Microbiol 14:1913–1928. https://doi.org/10.1111/j.1462-2920.2011.02657.x.
26. Ghafoor A, Hay ID, Rehm BHA. 2011. Role of exopolysaccharides in *Pseudomonas aeruginosa* biofilm formation and architecture. Appl Environ Microbiol 77:5238–5246. https://doi.org/10.1128/AEM.00637-11.
27. Ma L, Jackson KD, Landry RM, Parsek MR, Wozniak DJ. 2006. Analysis of *Pseudomonas aeruginosa* conditional Psl variants reveals roles for the Psl polysaccharide in adhesion and maintaining biofilm structure postattachment. J Bacteriol 188:8213–8221. https://doi.org/10.1128/JB.01202-06.
28. Borlee BR, Goldman AD, Murakami K, Samudrala R, Wozniak DJ, Parsek MR. 2010. *Pseudomonas aeruginosa* uses a cyclic-di-GMP-regulated adhesin to reinforce the biofilm extracellular matrix. Mol Microbiol 75:827–842. https://doi.org/10.1111/j.1365-2958.2009.06991.x.
29. Colley B, Dederer V, Carnell M, Kjelleberg S, Rice SA, Klebensberger J. 2016. SiaA/D Interconnects c-di-GMP and RsmA aignaling to coordinate cellular aggregation of *Pseudomonas aeruginosa* in response to environmental conditions. Front Microbiol 7:179. https://doi.org/10.3389/fmicb.2016.00179.
30. Kragh KN, Alhede M, Rybtke M, Stavnsberg C, Jensen PO, Tolker-Nielsen T, Whiteley M, Bjarnsholt T. 2017. Inoculation method could impact the outcome of microbiological experiments. Appl Environ Microbiol 84:e02264-17. https://doi.org/10.1128/AEM.02264-17.
31. Irie Y, Borlee BR, O'Connor JR, Hill PJ, Harwood CS, Wozniak DJ, Parsek MR. 2012. Self-produced exopolysaccharide is a signal that stimulates biofilm formation in *Pseudomonas aeruginosa*. Proc Natl Acad Sci U S A 109:20632–20636. https://doi.org/10.1073/pnas.1217993109.
32. Chua SL, Sivakumar K, Rybtke M, Yuan MJ, Andersen JB, Nielsen TE, Givskov M, Tolker-Nielsen T, Cao B, Kjelleberg S, Yang L. 2015. C-di-GMP regulates Pseudomonas aeruginosa stress response to tellurite during both planktonic and biofilm modes of growth. Sci Rep 5:10052. https://doi.org/10.1038/srep10052.
33. Chew SC, Kundukad B, Seviour T, van der Maarel JRC, Yang L, Rice SA, Doyle P, Kjelleberg S. 2014. Dynamic remodeling of microbial biofilms by functionally distinct exopolysaccharides. mBio 5:e01536-14. https://doi.org/10.1128/mBio.01536-14.
34. Armbruster CR, Wolter DJ, Mishra M, Hayden HS, Radey MC, Merrihew G, MacCoss MJ, Burns J, Wozniak DJ, Parsek MR, Hoffman LR. 2016. Staphylococcus aureus protein A mediates interspecies interactions at the cell surface of Pseudomonas aeruginosa. mBio 7:e00538-16. https://doi.org/10.1128/mBio.00538-16.
35. Billings N, Millan M, Caldara M, Rusconi R, Tarasova Y, Stocker R, Ribbeck K. 2013. The extracellular matrix component Psl provides fast-acting antibiotic defense in *Pseudomonas aeruginosa* biofilms. PLoS Pathog 9:e1003526. https://doi.org/10.1371/journal.ppat.1003526.
36. Periasamy S, Nair HAS, Lee KWK, Ong J, Goh JQJ, Kjelleberg S, Rice SA. 2015. Pseudomonas aeruginosa PAO1 exopolysaccharides are important for mixed species biofilm community development and stress tolerance. Front Microbiol 6:851. https://doi.org/10.3389/fmicb.2015.00851.

37. Wirtz D. 2009. Particle-tracking microrheology of living cells: principles and applications. Annu Rev Biophys 38:301–326. https://doi.org/10.1146/annurev.biophys.050708.133724.
38. Guigas G, Kalla C, Weiss M. 2007. Probing the nanoscale viscoelasticity of intracellular fluids in living cells. Biophys J 93:316–323. https://doi.org/10.1529/biophysj.106.099267.
39. Yang YL, Lin J, Kaytanli B, Saleh OA, Valentine MT. 2012. Direct correlation between creep compliance and deformation in entangled and sparsely crosslinked microtubule networks. Soft Matter 8:1776–1784. https://doi.org/10.1039/C2SM06745E.
40. Langley NR, Polmanteer KE. 1974. Relation of elastic modulus to crosslink and entanglement concentrations in rubber networks. J Polym Sci B Polym Phys 12:1023–1034. https://doi.org/10.1002/pol.1974.180120601.
41. Ruthardt N, Lamb DC, Brauchle C. 2011. Single-particle tracking as a quantitative microscopy-based approach to unravel cell entry mechanisms of viruses and pharmaceutical nanoparticles. Mol Ther 19:1199–1211. https://doi.org/10.1038/mt.2011.102.
42. Reverey JF, Jeon JH, Bao H, Leippe M, Metzler R, Selhuber-Unkel C. 2015. Superdiffusion dominates intracellular particle motion in the supercrowded cytoplasm of pathogenic *Acanthamoeba castellanii*. Sci Rep 5:11690. https://doi.org/10.1038/srep11690.
43. Mashburn LM, Jett AM, Akins DR, Whiteley M. 2005. *Staphylococcus aureus* serves as an iron source for *Pseudomonas aeruginosa* during *in vivo* coculture. J Bacteriol 187:554–566. https://doi.org/10.1128/JB.187.2.554-566.2005.
44. Imperi F, Tiburzi F, Visca P. 2009. Molecular basis of pyoverdine siderophore recycling in *Pseudomonas aeruginosa*. Proc Natl Acad Sci U S A 106:20440–20445. https://doi.org/10.1073/pnas.0908760106.
45. Yang L, Nilsson M, Gjermansen M, Givskov M, Tolker-Nielsen T. 2009. Pyoverdine and PQS mediated subpopulation interactions involved in *Pseudomonas aeruginosa* biofilm formation. Mol Microbiol 74:1380–1392. https://doi.org/10.1111/j.1365-2958.2009.06934.x.
46. Radlinski L, Rowe SE, Kartchner LB, Maile R, Cairns BA, Vitko NP, Gode CJ, Lachiewicz AM, Wolfgang MC, Conlon BP. 2017. *Pseudomonas aeruginosa* exoproducts determine antibiotic efficacy against *Staphylococcus aureus*. PLoS Biol 15:e2003981. https://doi.org/10.1371/journal.pbio.2003981.
47. Flemming HC, Wingender J. 2010. The biofilm matrix. Nat Rev Microbiol 8:623–633. https://doi.org/10.1038/nrmicro2415.
48. Jäger-Zürn I, Grubert M. 2000. Podostemaceae depend on sticky biofilms with respect to attachment to rocks in waterfalls. Int J Plant Sci 161:599–607. https://doi.org/10.1086/314292.
49. Birjiniuk A, Billings N, Nance E, Hanes J, Ribbeck K, Doyle PS. 2014. Single particle tracking reveals spatial and dynamic organization of the *Escherichia coli* biofilm matrix. New J Phys 16:085014. https://doi.org/10.1088/1367-2630/16/8/085014.
50. Klebensberger J, Birkenmaier A, Geffers R, Kjelleberg S, Philipp B. 2009. SiaA and SiaD are essential for inducing autoaggregation as a specific response to detergent stress in *Pseudomonas aeruginosa*. Environ Microbiol 11:3073–3086. https://doi.org/10.1111/j.1462-2920.2009.02012.x.
51. Chen Y, Yuan M, Mohanty A, Yam JK, Liu Y, Chua SL, Nielsen TE, Tolker-Nielsen T, Givskov M, Cao B, Yang L. 2015. Multiple diguanylate cyclase-coordinated regulation of pyoverdine synthesis in *Pseudomonas aeruginosa*. Environ Microbiol Rep 7:498–507. https://doi.org/10.1111/1758-2229.12278.
52. Lin Chua S, Liu Y, Li Y, Jun Ting H, Kohli GS, Cai Z, Suwanchaikasem P, Kau Kit Goh K, Pin Ng S, Tolker-Nielsen T, Yang L, Givskov M. 2017. Reduced intracellular c-di-GMP content increases expression of quorum sensing-regulated genes in *Pseudomonas aeruginosa*. Front Cell Infect Microbiol 7:451. https://doi.org/10.3389/fcimb.2017.00451.
53. Yang L, Hu Y, Liu Y, Zhang J, Ulstrup J, Molin S. 2011. Distinct roles of extracellular polymeric substances in *Pseudomonas aeruginosa* biofilm development. Environ Microbiol 13:1705–1717. https://doi.org/10.1111/j.1462-2920.2011.02503.x.
54. Lesic B, Rahme LG. 2008. Use of the lambda Red recombinase system to rapidly generate mutants in *Pseudomonas aeruginosa*. BMC Mol Biol 9:20. https://doi.org/10.1186/1471-2199-9-20.
55. Lagendijk EL, Validov S, Lamers GE, de Weert S, Bloemberg GV. 2010. Genetic tools for tagging Gram-negative bacteria with mCherry for visualization in vitro and in natural habitats, biofilm and pathogenicity studies. FEMS Microbiol Lett 305:81–90. https://doi.org/10.1111/j.1574-6968.2010.01916.x.
56. Toledo-Arana A, Merino N, Vergara-Irigaray M, Débarbouillé M, Penadés JR, Lasa I. 2005. *Staphylococcus aureus* develops an alternative, *ica*-independent biofilm in the absence of the *arlRS* two-component system. J Bacteriol 187:5318–5329. https://doi.org/10.1128/JB.187.15.5318-5329.2005.
57. Heydorn A, Nielsen AT, Hentzer M, Sternberg C, Givskov M, Ersboll BK, Molin S. 2000. Quantification of biofilm structures by the novel computer program COMSTAT. Microbiology 146:2395–2407. https://doi.org/10.1099/00221287-146-10-2395.
58. Vorregaard M. 2008. Comstat2—a modern 3D image analysis environment for biofilms. Technical University of Denmark, Kongens Lyngby, Denmark.
59. Curran-Everett D, Taylor S, Kafadar K. 1998. Fundamental concepts in statistics: elucidation and illustration. J Appl Physiol (1985) 85:775–786. https://doi.org/10.1152/jappl.1998.85.3.775.
60. Flohr RC, Blom CJ, Rainey PB, Beaumont HJ. 2013. Founder niche constrains evolutionary adaptive radiation. Proc Natl Acad Sci U S A 110:20663–20668. https://doi.org/10.1073/pnas.1310310110.
61. Schneider CA, Rasband WS, Eliceiri KW. 2012. NIH Image to ImageJ: 25 years of image analysis. Nat Methods 9:671–675. https://doi.org/10.1038/nmeth.2089.
62. Sbalzarini IF, Koumoutsakos P. 2005. Feature point tracking and trajectory analysis for video imaging in cell biology. J Struct Biol 151:182–195. https://doi.org/10.1016/j.jsb.2005.06.002.
63. Tarantino N, Tinevez JY, Crowell EF, Boisson B, Henriques R, Mhlanga M, Agou F, Israel A, Laplantine E. 2014. TNF and IL-1 exhibit distinct ubiquitin requirements for inducing NEMO-IKK supramolecular structures. J Cell Physiol 204:231–245. https://doi.org/10.1083/jcb.201307172.
64. Holloway BW, Morgan AF. 1986. Genome organization in *Pseudomonas*. Annu Rev Microbiol 40:79–105. https://doi.org/10.1146/annurev.mi.40.100186.000455.